

In vivo OCT microangiography of rodent iris

Woo June Choi,^{1,†} Zhongwei Zhi,^{1,†} and Ruikang K. Wang^{1,2,*}

¹Department of Bioengineering, University of Washington, Seattle, Washington 98195, USA

²Department of Ophthalmology, University of Washington, Seattle, Washington 98195, USA

*Corresponding author: wangrk@uw.edu

Received January 7, 2014; revised March 20, 2014; accepted March 21, 2014;
posted March 21, 2014 (Doc. ID 204210); published April 11, 2014

We report on the functional optical coherence tomography (OCT) imaging of iris tissue morphology and microcirculation in living small animals. Anterior segments of healthy mouse and rat eyes are imaged with high-speed spectral domain OCT (SD-OCT) utilizing ultrahigh sensitive optical microangiography (UHS-OMAG) imaging protocol. 3D iris microvasculature is produced by the use of an algorithm that calculates absolute differences between the amplitudes of the OCT interframes. We demonstrate that the UHS-OMAG is capable of delineating iris microvascular beds in the mouse and rat with capillary-level resolution. Furthermore, the fast imaging speed enables dynamic imaging of iris micro-vascular response during drug-induced pupil dilation. We believe that this OCT angiographic approach has a great potential for *in situ* and *in vivo* monitoring of the microcirculation within iris tissue beds in rodent disease models that have microvascular involvement. © 2014 Optical Society of America
OCIS codes: (170.4500) Optical coherence tomography; (170.4470) Ophthalmology; (170.2655) Functional monitoring and imaging.

<http://dx.doi.org/10.1364/OL.39.002455>

In ophthalmic research, rodent models are essential for improved understanding of the eye disease process due to their availability for genetic manipulation [1–3]. The small animals have particularly contributed to the evaluation of pathophysiology of ocular vascular diseases such as glaucoma because disorders in the eye circulation (e.g., angiogenesis and ischemia) as early symptoms of the ocular vascular diseases are well-characterized in the transgenic rodent eyes [4]. Currently, intraocular vasculature in disease models is mainly examined by the use of standard fluorescein angiography (FA) [5] and confocal laser scanning microscopy [6] that commonly require invasive injection of contrast agents (e.g., fluorescein and indocyanine green). Alternatively, label-free ocular vascular imaging has been demonstrated by photoacoustic microscopy (PAM) by using intrinsic hemoglobin absorption contrast of red blood cells (RBCs), mapping major vessels in retina of rats *in vivo* [7,8]. On the other hand, by utilizing dynamic optical scattering from moving RBCs within patent vessels, recent developments of optical coherence tomography (OCT) based microangiography have also offered great potential in delineating the retinal microvasculature in living mice and rats without the administration of contrast agents [e.g., 9,10].

Although there are increased interests in using endogenous-based angiographic methods to image retinal microvasculature within posterior segment in rodents, microcirculation in the anterior segment has barely been explored. In the anterior segment, especially, the iris tissue bed would be a desirable site to monitor the progression of the ocular vascular diseases. For example, it is well known that iris neovascularization (rubeosis iris) is directly associated with the disease process in the retina, leading to secondary glaucoma, followed by vision loss [11]. Recently, optical resolution PAM (OR-PAM) has showed the feasibility of label-free iris vascular imaging in mice [12,13]. Despite the high imaging quality it offers, this approach is currently limited to a long image-acquisition time (up to 2 h) and physical contact of a water bath with cornea, which may hamper viability of the rodent and make it difficult for use in longitudinal

measurement in individual animals. Here we report on the application of OCT microangiography to the rodent's iris *in vivo*. This technique enables fast 3D image acquisition within a few seconds for living animals without physical contact, warranting reliable vascular measurement for longitudinal investigation of vascular ocular disease progression or therapeutic effects.

To obtain the iris vasculature in rodent eyes, we employed a home-built high-speed spectral-domain OCT (SD-OCT) system as shown in Fig. 1, similar to the one depicted in our previous work [14]. In brief, a broadband super-luminescent diode (LS2000B, center wavelength = 1340 nm, 3 dB spectral bandwidth = 110 nm, Thorlabs Inc.) was used as the light source. Light from the laser was split into a reference arm and a sample arm by a 10:90 fiber coupler. In the sample arm, a 10× telecentric objective (LSM02, effective focal length = 18 mm, Thorlabs Inc.) formed a beam spot having a diameter of ~7 μm in focus. The average power of the incident beam was 1.9 mW. The beam spot was raster-scanned across the sample by a pair of X-Y galvo scanners (6210H, Cambridge Technology) placed in the back focal plane of the objective. Retro-reflected lights from each

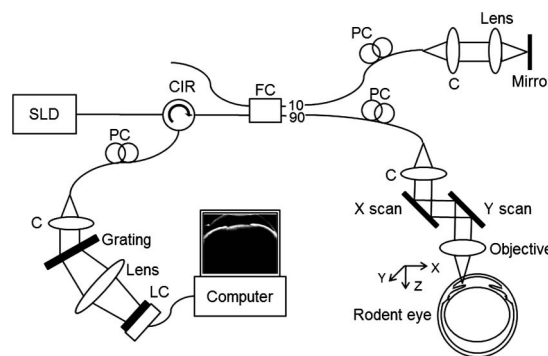


Fig. 1. Schematic of the high-speed SD OCT system for *in vivo* vascular imaging of a rodent eye. SLD, superluminescent diode; CIR, circulator; FC, fiber coupler; PC, polarization controller; C, collimator; LC, line CCD camera.

arm were recombined with the same coupler, and the resulting interference signal was detected by a home-built fast spectrometer providing a spectral resolution of 0.141 nm and a maximum A-line scan rate of 92 kHz. The measured sensitivity and axial resolution of the system were 100 dB (at 0.5 mm below the zero delay line) and $\sim 7 \mu\text{m}$ in air, respectively.

To demonstrate the feasibility of using OCT microangiography to delineate iris microcirculation *in vivo*, we used rodent animals of a C57BL/6 mouse (male, 2–3 months old, ~ 23 g weight) and a brown Norway BN/091 rat (male, eight months old, ~ 300 g weight) in this study. The experiments were performed under a laboratory animal protocol approved by the Animal Care and Use Committee of University of Washington. During imaging, the animals were anesthetized by inhalation of a mixture of 1.5% isoflurane, 80% air, and 20% oxygen and placed onto a custom-made stage where the rodent eye of interest was positioned beneath the objective. Anesthesia status was maintained by a breathing mask on the stage throughout the experiment. The body temperature of the animals was kept at 37°C with a temperature-controlled heating pad. A 0.5% artificial teardrop (Alcon Inc.) was applied to the eye surface to prevent cornea from dehydration. Iris structure to be imaged was carefully positioned within the depth of focus (DOF) of the scanning probe beam as monitored by real-time OCT imaging on the fly at computer monitor.

For vascular imaging of both rodent models, we utilized the imaging protocol of ultrahigh sensitive optical microangiography (UHS-OMAG) as one of capillary-resolved OCT microangiography techniques [15]. In this protocol, we captured 500 A-lines for each B-frame (in x axis) and 2000 cross sections (in y axis) with five repetitions in each location (400 locations in total) at a B-scan rate of 180 frames per second. Such scanning covered a field of view (FOV) of $3 \text{ mm} \times 3 \text{ mm}$. The total acquisition time of the 3D OCT data ($500(X) \times 2000(Y) \times 1024(Z)$ voxels) was ~ 10 s, which is tolerable for the anesthetized small animals. From the acquired 3D OCT data, the average of absolute differences between the amplitudes of the OCT interframes at each location in the y axis produced one cross-sectional image, depicting functional vessels within the cross section. The collection of cross-sectional images at all locations formed a 3D volume of iris tissue microcirculation.

Imaging result for the mouse anterior eye is shown in Fig. 2, where the panel (a) gives a representative cross-sectional OCT image, providing typical tissue structures in the anterior segment of the mouse eye, including cornea, crystalline lens, and iris. The top portion of the cornea crossed over the zero-delay line is flipped in the

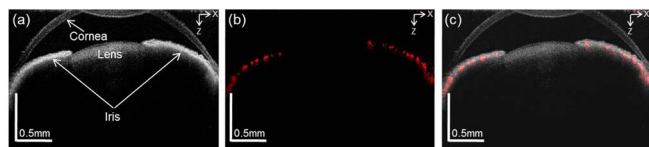


Fig. 2. *In vivo* OCT microangiography of anterior eye in a healthy C57BL/6 mouse. (a) Representative cross-sectional OCT image. (b) Corresponding blood flow image. (c) Merged view of (a) and (b). Image area is $3.0 \text{ mm}(X) \times 1.39 \text{ mm}(Z)$.

image due to the well-known mirror artifact in Fourier domain OCT. The corresponding microvascular image is red color-mapped in Fig. 2(b), in which small vessel signals are localized only within the iris rather than the avascular cornea and lens. This is evident from the merged view [Fig. 2(c)] of Figs. 2(a) and 2(b). A 3D volumetric image can then be produced by collecting such cross-sectional images sequentially at all the locations in the y axis. Figure 3(a) is a maximum-intensity projection (MIP) view of the 3D image of the mouse anterior eye where the removal of the cornea structure was carefully taken from the 3D OCT structures of the eye for better visualization of the iris tissue. The *en face* projection view exhibits a diaphragm-shaped iris with central opening, pupil, and relatively opaque posterior lens below the pupil. Figure 3(b) shows the corresponding MIP view of 3D cross-sectional microvascular images, representing a functional micro-circulatory network perfused within iris tissue beds. Visually, the iris microvasculature consists of radial branches of small vessels and capillaries in a relatively linear pattern. Major arterial circles (MICs) (open arrows) are observed around the iris root and the ciliary body from which small arteries branch out and extend toward the pupillary margin. Some of the MICs at the iris periphery appear to be slightly blurred. This is due to the fact that the focal plane in the experiment was carefully positioned at the middle way of iris, leading to the MICs out of focus below the focal plane. In the pupillary margin, the lesser iris circles (LICs) with corn-shaped arcades (arrow heads) is clearly visible, bridging adjacent vascular networks. From the overlaid image in Fig. 3(c), the iris vasculature is co-registered with the iris structure. Our finding is quite similar to the mouse angiographic results produced by the photoacoustic imaging microscopy [12,13], where, however, the light absorption of hemoglobin presented in the blood is used as the imaging contrast mechanism. In contrast, UHS-OMAG (or

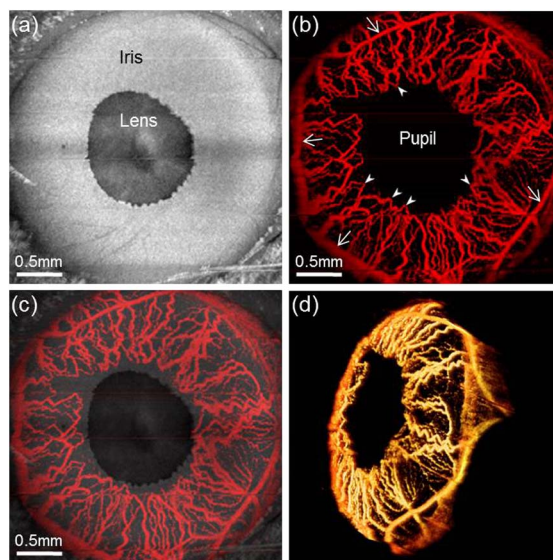


Fig. 3. *In vivo* OCT microangiography of anterior eye in a healthy C57BL/6 mouse. (a) Maximum intensity projection (MIP) view [$3 \text{ mm}(X) \times 3 \text{ mm}(Y)$] of the 3D OCT images and (b) corresponding microvascular MIP image. (c) Overlaid image of (a) and (b). (d) 3D rendered iris vasculature (Media 1).

OCT-based angiography in general) here utilizes endogenous optical scattering due to moving RBCs within tissue beds as the contrast mechanism.

In vivo iris imaging of rat using UHS-OMAG is demonstrated in Fig. 4. Due to the limited FOV of the system used in this study (currently $3\text{ mm} \times 3\text{ mm}$), shown in Figs. 4(a) and 4(b) are, respectively, the OCT structural and OMAG vascular MIP images of the upper-right portion of the rat anterior eye. The rat pupil as seen [Fig. 4(a)] is contracted because the experiment was performed under relatively bright ambient illumination. The iris microvascular network of the rat [Fig. 4(b)] represents densely packed radial small vessels toward the center of pupil, while appearing rather irregularly less packed when approaching the iris root. A single branch of a long posterior ciliary artery (LPCA) [arrows in Fig. 4(b)] traveling almost perpendicular to the radial vessels is seen in the vicinity of the iris root [16]. In order to resolve individual vessels, we performed an additional experiment by reducing the system FOV to $1.75\text{ mm} \times 1.75\text{ mm}$ while keeping the scanning protocol described above unchanged. Shown in Figs. 4(c) and 4(d) are, respectively, the MIP structural and vascular images resulted from the reduced FOV scanning, demonstrating improved ability to visualize the anatomical and vascular features within iris tissue beds. Based solely on endogenous optical scattering signals from moving RBCs within patent blood vessels without the use of any contrast agents, the capability of functional UHS-OMAG imaging of iris tissue beds in both rat and mice can be particularly useful in the investigation of vascular involvements in eye diseases that may affect the iris.

High-speed UHS-OMAG imaging enables temporal measurements of dynamic vascular responses of the iris to stimulus (including both passive and active). To assess

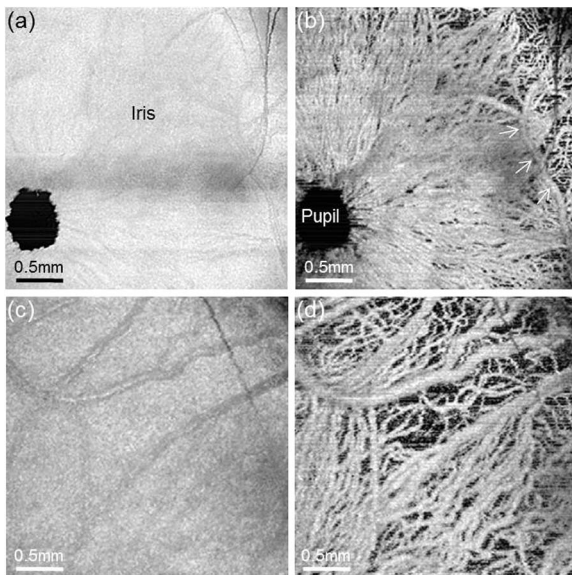


Fig. 4. *In vivo* OCT microangiography of anterior eye in a healthy BN/091 rat. (a) Maximum intensity projection (MIP) image [$3\text{ mm}(X) \times 3\text{ mm}(Y)$] of 3D OCT images and (b) corresponding microvascular MIP image. (c) and (d) MIP images [$1.75\text{ mm}(X) \times 1.75\text{ mm}(Y)$] of OCT structure and vascular structure obtained around the iris root of the same rat eye, respectively.

its feasibility, we imaged a normal C57BL/6 mouse eye with drug-induced pupil dilation (mydriasis). A drop of 1% tropicamide ophthalmic solution was applied onto the mouse cornea to dilate the pupil for a short period. The imaging was performed in normal ambient (room) illumination. Figure 5 shows the time-lapsed changes of the iris vessel network of the mouse eye during pupil dilation: (a) baseline, (b) right after, (c) 1 min after, (d) 2 min after the application of the drug, respectively. The radial iris blood vessels at the baseline [Fig. 5(a)] are gradually becoming tortuous after the drug application [see Figs. 5(c) and 5(d)]. On the other hand, the vascular network of the pupillary margin is stretched out as the pupil aperture enlarges [arrowheads in Figs. 5(c) and 5(d)]. This can be explained by the fact that drug-induced sympathetic stimulation causes the contraction of the dilator muscle, leading to possible compression of the radial vessels [16,17]. The iris vessel tortuosity against the increase of the pupil area is quantified and plotted in Fig. 5(d) in which the vessel tortuosity was calculated by applying a fractal dimension method [18] to each vascular projection image. The quantification of the dynamic vessel tortuosity, due to a stimulus would be beneficial for characterizing the functionality as well as abnormality of the iris, thus may provide improved understanding of the eye diseases that involve iris tissue beds, such as glaucoma, uveitis, scleritis, anterior ocular tumor, etc.

Although we have demonstrated that the iris microcirculation in living rodents can be imaged within a

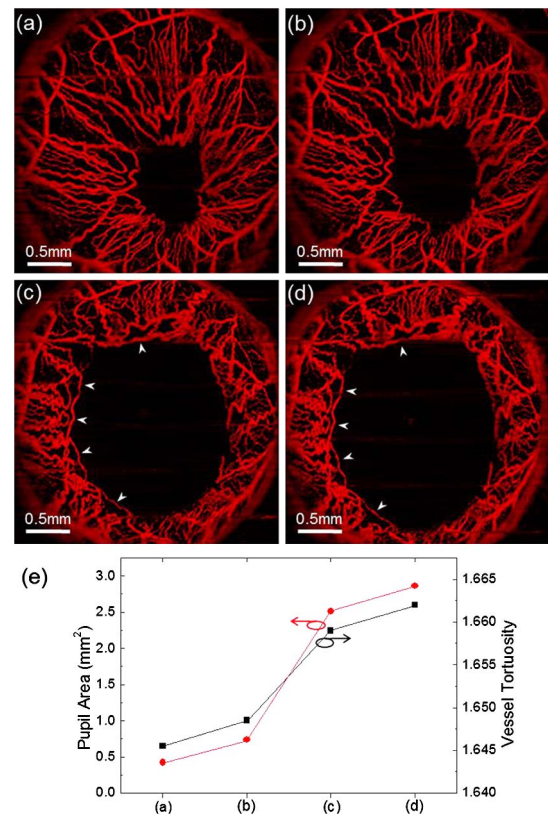


Fig. 5. Dynamic iris vascular response of the healthy C57BL/6 mouse anterior eye to the drug-induced pupil dilation: (a) baseline, (b) right after, (c) 1 min after, (d) 2 min after the application of the drug. (e) The quantified iris vessel tortuosity and the pupil area during the pupil dilation of the mouse iris.

relatively short time scale (~ 10 s) using our current imaging system, the resulted vascular images were still subject to physiological motion due to respiration (55/min for the anesthetized rat) and heartbeat, introducing regular pattern noises (artifacts) on the final vessel image. These imaging artifacts are clearly visible in the results presented here; for example, the regular horizontal stripes (caused by respiration) and saw-tooth appearance in the edge of pupil (due to heart beat). Post-processing of high-pass Fourier filtering is a good choice to minimize the horizontal artifacts on the vessel image for the current system (as we already included in our data-processing). Other approaches (for example, OCT image co-registration before the vascular mapping) should be explored in the future to minimize further the motion artifacts so that the iris microcirculation can be evaluated and quantified more accurately. The system used in the current study had an imaging speed of 92,000 A-lines per second, which required an imaging time of 12 s to acquire a 3D dataset for OCT angiography. Clearly this is the main cause of the resulting bulk tissue motion artifacts. Improving the imaging speed of the system can be an alternative approach to eliminate the possible tissue motion artifacts. OCT systems with ultra-high imaging speed are currently being developed; for example, swept-source OCT system employing VCSEL light source, which is reported to deliver an imaging speed of a few MHz for 4D volumetric imaging [19] that may remove artifacts owing to physiological motion. Such high-speed imaging system may be particularly important if 4D (3D volume + time) imaging of microvascular response to certain insults (either stimulation or injury) is required in the investigation. However, one possible drawback when using an MHz imaging system to image tissue micro-circulation is that the scattering signals from moving RBCs may be changed relatively slowly (or even frozen) within the adjacent B-scans, leading to decreased imaging contrast of the tissue microcirculation. Such possible consequence deserves further investigation.

In summary, we have demonstrated *in vivo* OCT microangiography of the rodent iris. High-speed OCT has enabled noncontact, fast 3D image acquisition in the rodent eyes, providing comprehensive 3D iris vascular networks as well as possible 4D dynamic microangiography of the functional response of the rodent iris to a drug stimulus. Therefore, the anterior OCT microangiography may promise a useful tool for the *in vivo* monitoring of the iris microcirculation changes in ocular vascular disease models in living rodents.

This work was supported in part by NIH R01EB009682, R01HL093140, R01EY024158, the Coulter Translational Research Partnership Program, Research to Prevent Blindness, and the Department of Bioengineering at the University of Washington. Dr. Wang is a recipient of Research to Prevent Blindness Innovative Ophthalmic Research Award.

†Authors contributed equally to the manuscript

References

1. R. S. Smith, N. L. Hawes, S. D. Kuhlmann, J. R. Heckenlively, B. Chang, T. H. Roderick, and J. P. Sundberg, *Investig. Ophthalmol. Vis. Sci.* **37**, 397 (1996).
2. J. Graw, *J. Genet.* **88**, 469 (2009).
3. B. Chang, N. L. Hawes, R. E. Hurd, J. Wang, D. Howell, M. T. Davisson, T. H. Roderick, S. Nusinowitz, and J. R. Heckenlively, *Vis. Neurosci.* **22**, 587 (2005).
4. L. M. Ittner, K. Schwerdtfeger, T. H. Kunz, R. Muff, K. Husmann, C. Grimm, F. Hafezi, K. S. Lang, M. O. Kurrer, J. Götz, W. Born, and J. A. Fischer, *Clinical Sci.* **114**, 49 (2008).
5. R. D'Amato, E. Wesolowski, and L. E. H. Smith, *Microvasc. Res.* **46**, 135 (1993).
6. M. R. Ritter, E. Aguilar, E. Banin, L. Schepcke, H. U. Jarvinen, and M. Friedlander, *Investig. Ophthalmol. Vis. Sci.* **46**, 3021 (2005).
7. S. Jiao, M. Jiang, J. Hu, A. Fawzi, Q. Zhou, K. K. Shung, C. A. Puliafito, and H. F. Zhang, *Opt. Express* **18**, 3967 (2010).
8. W. Song, Q. Wei, T. Liu, D. Kuai, J. M. Burke, S. Jiao, and H. F. Zhang, *J. Biomed. Opt.* **17**, 061206 (2012).
9. Z. Zhi, X. Yin, S. Dziennis, T. Wietecha, K. L. Hudkins, C. E. Alpers, and R. K. Wang, *Biomed. Opt. Express* **3**, 2976 (2012).
10. V. J. Srinivasan and H. Radhakrishnan, *J. Biomed. Opt.* **18**, 076025 (2013).
11. R. J. H. Smith, *Br. J. Ophthalmol.* **65**, 606 (1981).
12. S. Hu, B. Rao, K. Maslov, and L. V. Wang, *Opt. Lett.* **35**, 1 (2010).
13. B. Rao, L. Li, K. Maslov, and L. V. Wang, *Opt. Lett.* **35**, 1521 (2010).
14. L. Shi, J. Qin, and R. K. Wang, *J. Biomed. Opt.* **18**, 106015 (2013).
15. R. K. Wang, L. An, P. Francis, and D. Wilson, *Opt. Lett.* **35**, 1467 (2010).
16. H. M. Stauss, K. R. Rarick, K. M. Leick, J. W. Burkle, D. L. Rotella, and M. G. Anderson, *Am. J. Physiol. Regul. Integr. Comp. Physiol.* **300**, R1333 (2011).
17. P. Henkind, *Br. J. Ophthalmol.* **49**, 6 (1965).
18. R. Reif, J. Qin, L. An, Z. Zhi, S. Dziennis, and R. K. Wang, *Int. J. Biomed. Imaging* **2012**, 509783 (2012).
19. B. Potsaid, V. Jayaraman, J. G. Fujimoto, J. Jiang, P. J. S. Heim, and A. E. Cable, *Proc. SPIE* **8213**, 82130M (2012).